Powder Technology 444 (2024) 120044

Contents lists available at ScienceDirect

Powder Technology

journal homepage: www.journals.elsevier.com/powder-technology

Improving laser powder bed fusion processability of pure Cu through powder functionalization with Ag

Giorgia Lupi [a], Marcello Poulin [a], Federico Gobber [b], Marco Actis Grande [b], Riccardo Casati [a,*]

[a] Department of Mechanical Engineering, Politecnico di Milano, Via G. La Masa 34, 20156 Milano, MI, Italy
[b] Department of Applied Science and Technology, Politecnico di Torino, Viale T. Michel 5, 15121 Alessandria, Italy

HIGHLIGHTS

- Cu powder processability enhanced via Ag-coating in low-power near-IR LPBF system
- Heat treatment studies on powder to promotes diffusion and heterostructure formation
- Notable improvement in material density observed with Ag-coated powders
- Healing capability of Ag during last stages of solidification

GRAPHICAL ABSTRACT

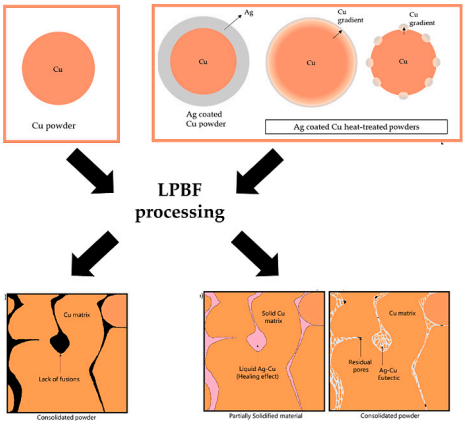

ARTICLE INFO

Keywords:
Coated metal powders
Powder functionalization
LPBF
Copper
Silver

ABSTRACT

The Laser Powder Bed Fusion (LPBF) manufacturing of dense Cu parts with near infrared conventional systems is still challenging due to the high reflectivity and thermal conductivity of the powder. In this paper, we investigate a novel approach to improve LPBF processability of Cu through the modification of particle surface properties. Pure Cu powders were coated with a thin layer of high-conductivity Ag by electrodeposition. The coated powder was also heat-treated at 500 °C and 600 °C to promote diffusion at the coating interface, producing different powder particle configurations. LPBF equipped with 200 W laser was used to produce bulk samples using pure Cu and Cu/Ag powder, which were comprehensively characterized by electron microscopy and X-ray diffraction. The Ag coating improved the material processability and density, forming a eutectic phase mixture able to heal pores and defects at the end of the solidification process.

* Corresponding author.
E-mail address: riccardo.casati@polimi.it (R. Casati).

https://doi.org/10.1016/j.powtec.2024.120044
Received 9 May 2024; Received in revised form 12 June 2024; Accepted 2 July 2024
Available online 3 July 2024

1. Introduction

The Laser Powder Bed Fusion (LPBF) processability of Cu can pose significant challenges due to high near infrared (IR) laser reflectivity and high thermal conductivity [1,2]. The low penetration of the laser and the high thermal conductivity of Cu result in a quick dissipation into the metal of the energy put into the system during the scan, leading to the presence of lack-of-fusion defects, thus implying the production of parts that generally do not meet the standards of industry [3–6]. Accordingly, different methods have been proposed to produce fully dense and high-performance bulk materials, such as using high laser power and the utilization of lasers with different wavelengths (green or blue diode lasers) [7–9]. However, these kinds of lasers are less common and are not installed in most of the industrial systems. Another possible solution can be the modification of the original chemical composition of powder by adding proper alloying elements, which is often necessary to produce dense and crack-free structural parts [10–12]. Thus, the study of pre-alloyed Cu powders is extremely important to improve the laser processability [13–19]. As an example, Zhang et al. were able to process a pre-alloyed Cu—Cr powder and obtain samples with a relative density of 99.98%. After heat treatment, ultimate tensile strength of 468 MPa, yield strength of 377 MPa, elongation of 19%, and electrical conductivity of 98% IACS were achieved [20]. The Cu-15Ni-8Sn system has also been reported in the open literature. Components were manufactured by LPBF with a near full density of 99.4% by using laser power in the range of 220 to 340 W. The as-fabricated Cu-15Ni-8Sn alloy exhibited a yield strength of 522 MPa, an ultimate tensile strength of 653 MPa, and elongation of 17% [21]. Another approach to improve Cu processability involves the functionalization of the powder surface with thin coatings or discrete particles. Lindstrom et al. were able to coat Cu powders with Sn and Ni and process them through LPBF. The samples made from coated powders showed a lower amount of porosity compared to samples made from alloy powders of similar composition [22]. Hu et al. proposed to modify the laser reflectivity of Cu-Cr-Zr powder by applying a Y_2O_3 coating. The yield strength and ductility of Y_2O_3-Cu-Cr-Zr specimens were improved compared with those of Cu-Cr-Zr specimens [23]. Jadhav et al. produced a highly conductive and strong CuSn0.3 alloy processed via LPBF starting from a Sn-coated Cu powder. The application of only 0.28 wt% Sn coating significantly improved room temperature powder optical absorption by ~170% at the fiber laser wavelength (1080 nm) [24]. In the work of Zheng et al., Cu powders were coated with Ni to enhance the densification of Cu through LPBF. The Ni coating significantly decreased the high laser reflectivity of Cu powder and enabled the production of a denser material compared to pure Cu. The interface condition between the Ni coating and Cu powder was found to play a crucial role in the densification process. The solid solution of Ni in the surface Ni-alloyed powder maximized the contact area, reduced thermal resistance, and enhanced heat transfer efficiency, which eventually promoted the melting of Cu powder and eliminated the lack-of-fusion pores [25].

The objective of this study is to improve the processability of Cu by introducing an Ag layer onto the surface of powder particles and to evaluate the densification capability of Ag in the material processed through conventional 200 W near-IR LPBF. Despite its higher laser reflectivity, Ag was selected since it has high electrical conductivity, and it has been widely reported in the literature that CuAg alloys generally exhibit high strength and conductivity. Indeed, compared with other alloying elements, Ag has less influence on the conductivity of copper alloys [26–28]. Pure Cu powders were coated with a thin layer of Ag by electrodeposition and heat-treated according to different schedules to promote different coating configurations and to study their effect on the powder laser absorbance and processability. To assess the benefits of employing functionalized powders, samples were additionally printed using pure Cu and Cu—Ag alloy powder with the same average composition of the coated powder.

2. Experimental methods

Cu powder with D10 of 9.4 μm, D50 of 22.8 μm, and D90 of 45.3 μm was procured from Kimera International [29]. The Cu powder was coated with Ag by electroless deposition [30] by Kymera International using proprietary parameters. The coated powder showed a D10 of 9.7 μm, D50 of 22.6 μm, and D90 of 43.8 μm. The analysis of the chemical composition of the coated powder revealed a concentration of Ag of 4.3 wt%. The Ag-coated powder feedstocks were heat-treated according to different schedules in a vacuum furnace to study their effect on the processability of the powder. The heat treatment processes were conducted under vacuum conditions to minimize the possibility of oxidation of the coated powder. A batch of powder was treated at 500 °C for 1 h and a second batch at 600 °C for 1 h to promote the formation of different layer configurations.

In order to evaluate the processability of the Ag—Cu system, Cu-4.3%Ag powders were also produced using vacuum induction inert gas atomization (VIGA) on a PSI Hermiga 100/10 atomizer. A batch of powders was obtained starting from pure electrolytic Cu (99.99%) and pure Ag granules (99.9%). The pure elements were heated in an alumina crucible and then melted under a high purity 5.0 Ar shielding gas cover at an overpressure of 0.05 barg. The molten bath was held at a stable temperature of 1255 ± 5 °C for 15 min. Then, the overpressure was increased to 0.22 barg, and the melt was atomized with Ar at 42 bar. Finally, a gas-to-metal ratio of 1.35 was calculated. Throughout the entire powder production process, the amount of oxygen in the atomization chamber was monitored using a Zircona probe sensor (Rapidox 1100). The oxygen content ranged from 0.005%wt immediately after atomization to 0.009%wt before unloading the gas-atomized powders.

The powders were sieved to achieve a particle size distribution (PSD) of 20–63 μm, suitable for the LPBF process. A laboratory sieve shaker was used with three 200 mm diameter sieves (20 μm, 63 μm, and 120 μm), and 0.5 kg of powder was added for each run. Laser granulometry (Malvern Mastersizer 3000) measured the prealloyed Cu—Ag powders, which had a D10 of 26.8 μm, a D50 of 41.2 μm, and a D90 of 63.0 μm. The light element content was measured using the inert gas fusion technique (Leco ONH 836); 0.024 ± 0.002%wt O, 0.058 ± 0.003% N, and 2.68 ± 0.02 ppm H were reported out of three sampling. The powders were stored under inert Ar gas, and silica gel bags were added to prevent moisture absorption.

A Renishaw AM250 equipped with a Reduced Build Volume (RBV) module was used to print cylindrical samples having a diameter of 20 mm and a height of 5 mm. After the thorough optimization of process parameters (not reported in this manuscript), the optimal combination of parameters has been identified and listed in Table 1.

The investigation of the morphology of the different powder feedstocks was accomplished with a Field Emission Scanning Electron Microscope (FE-SEM) model Zeiss Sigma 500 equipped with energy dispersive X-ray analysis (EDX). To evaluate the coating thickness, high-magnification SEM images of different cross-sections from the various powder feedstocks were analyzed using ImageJ software.

X-ray diffraction (XRD) analyses were performed on powder feedstocks with a Rigaku SmartLab diffractometer employing Cu Kα radiation. The data were obtained in the diffraction angle range $20° \leq 2\theta \leq 80°$, with a step width of 0.01° and a velocity of 1°/min. XRD analysis has been used to evaluate the effective diffusion of Cu in the Ag layer after performing ad-hoc heat-treatment on the powder feedstocks.

Table 1
Process parameters use to print the samples.

Laser power	200 W
Time of exposure	140 μs
Point distance	80 μm
Hatch distance	130 μm
Layer thickness	30 μm

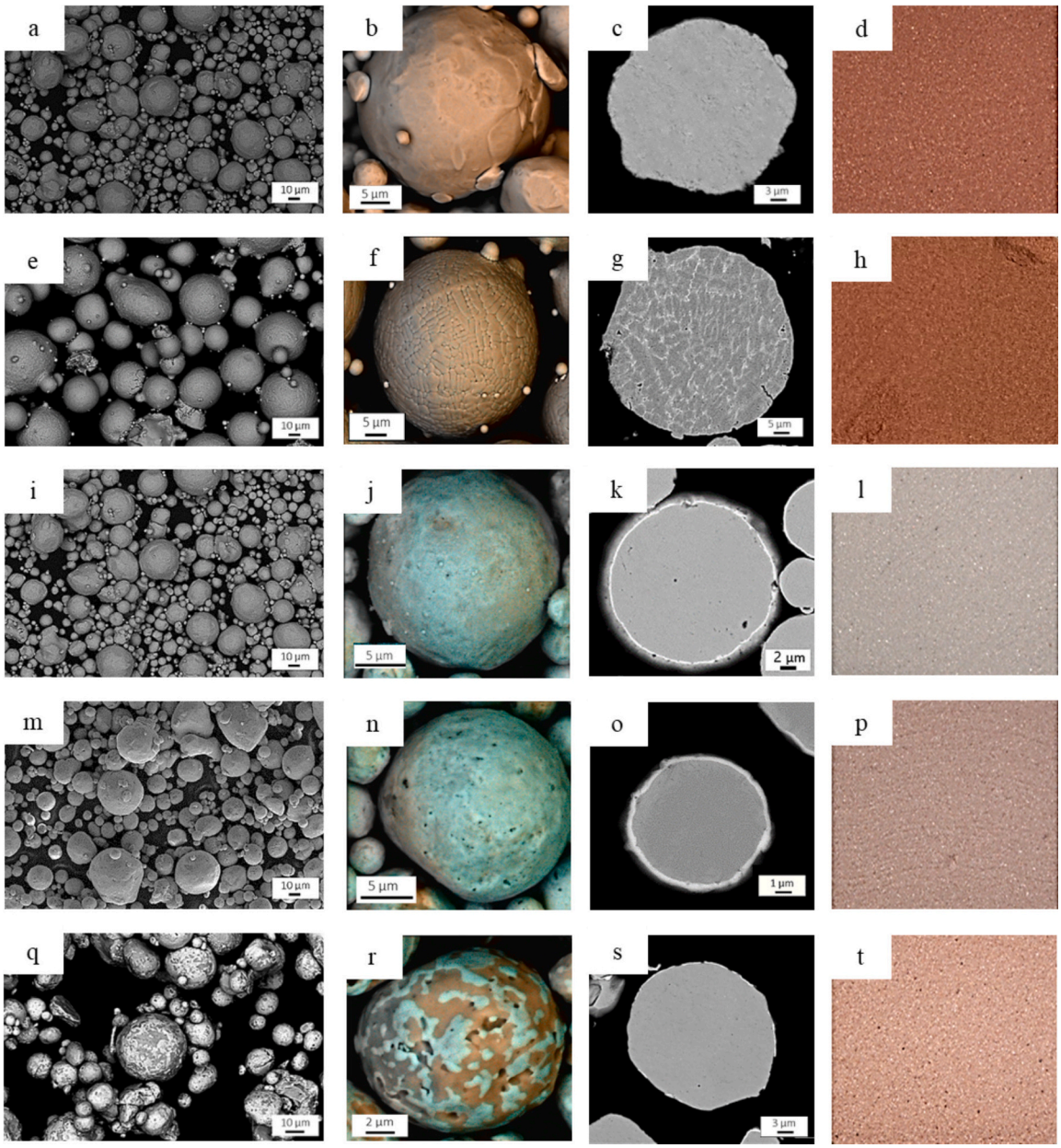

Fig. 1. SEM images, EDX elemental maps and picture of a),b),c),d) pure copper powder, e),f),g),h) Cu-4.3%Ag alloy powder, i),j),k),l) Ag coated Cu powder, m),n), o),p) Ag coated Cu powder heat-treated at 500 °C for 1 h, q),r),s),t) Ag coated Cu powder heat-treated at 600 °C for 1 h powder. In EDX maps, Cu and Ag are represented in orange and light blue, respectively. (For interpretation of the references to color in this figure legend, the reader is referred to the web version of this article.)

The absorbance of the different powder batches has been analyzed through a UV–Vis spectrophotometer UV-2600 (Shimadzu) equipped with the Integrating Sphere Attachment using a barium sulphate reference. The powder samples were mixed prior to being placed in the silica cuvettes, which were used as loading supports for the analysis.

The analysis of microstructures of bulk samples was performed by a light optical microscope (LOM) and SEM. Bulk samples for metallography were prepared following common grinding and polishing procedures. Image analysis with ImageJ software was performed to evaluate the relative density of the bulk samples.

3. Results

3.1. Powder characterization

The various powder feedstocks were analyzed with SEM, and the corresponding images are presented in Fig. 1. For each powder feedstock, the figure includes SEM images at low magnification showing the powder, EDX elemental maps, and high-magnification images of the cross-sections to better study the Ag coating. Additionally, Fig. 1 also includes pictures of the visual inspection of the different powder feedstocks, showing color changes following coating procedure and the heat treatments. Specifically, Fig. 1 show the pure Cu powder, the Cu-4.3%Ag alloy powder, the as-received Cu powder coated with the Ag layer, and the two Ag coated powder heat treated at 500 °C and 600 °C. In particular, it is possible to observe that the morphology of the Cu powder remains unchanged after the coating process and the heat-treatment at 500 °C. The heat-treatment at 600 °C revealed able to create discrete structure, leaving some surface regions without Ag coating.

To evaluate the effective diffusion of Cu more systematically, XRD analyses were conducted on the Ag-coated powder in both its as-received state and after heat treatment at 500 °C and 600 °C. The results are reported in Fig. 2, focusing on the diffractogram section within angles $37.5° \leq 2\theta \leq 39°$, including the diffraction peak of the (111) plane. The treatment led to a peak shift toward higher angles and to a peak asymmetry. Additionally, laser absorbance of the powders in different configurations was analyzed, with results presented in Fig. 3 as a function of wavelength. The coating has a significant effect on powder reflectivity up to a wavelength of 650 nm, but not at 1080 nm (see the dashed line in the diagram), i.e. the corresponding wavelength of the laser that was employed for processing the powders in this study.

3.2. Bulk characterization

Representative LOM images of the cross section of the bulk material

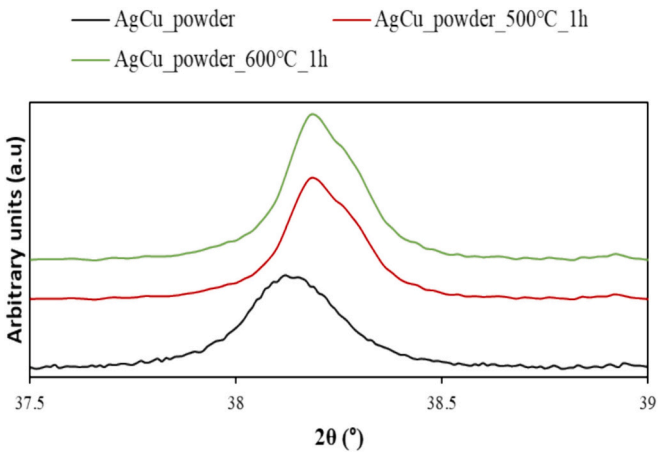

Fig. 2. XRD patterns of the Ag 111 peak visible at 38° for the Ag coated powders.

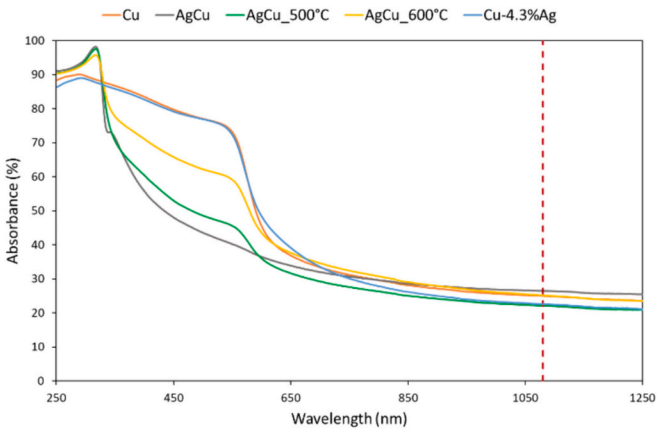

Fig. 3. Absorptivity measurements on the different powder feedstocks. The dashed line corresponds to the wavelength of 1080 nm, i.e. the characteristic wavelength of the laser used to print the sample in this study.

obtained with the different powder feedstocks are reported in Fig. 4. Bulk densities were determined by examining the cross-section of each sample through optical microscope. The relative densities of the samples were calculated with ImageJ software, and the results are displayed in Fig. 4.f. Notably, samples printed with functionalized powders and Cu-4.3%Ag alloy powder exhibited higher bulk relative densities compared to pure Cu samples, indicating an enhancement in the material processability. The printed Cu powder achieved low density level (93.4 ± 0.8%), partial melting of the material was induced by the laser and original powder particles are still visible. The continuity of the metal matrix is interrupted by several very thin discontinuities due to the partial melting of the material, i.e. lack-of-fusion defects (Fig. 4.a). The Cu-4.3%Ag samples achieved higher density (98.2 ± 0.4%), but the same discontinuities between partially melted powder particles are still visible (Fig. 4.b). The as received coated powder showed a better behavior, higher density value was achieved (99.0 ± 0.1%), and more importantly, no discontinuities of the metal matrix were noticeable (Fig. 4.c). A similar result was achieved with the coated powder treated at 500 °C (99.1 ± 0.4%), whereas slightly lower density value was achieved with powder treated at 600 °C (98.4 ± 0.3%) (Fig. 4.d and Fig. 4.e).

To further investigate on the mechanism of densification, SEM analysis of the microstructure was conducted, and the results are depicted in Fig. 5 and Fig. 6. Fig. 5.a presents SEM image of the pure Cu samples, revealing the presence of lack-of-fusion defects. Inspection at higher magnification revealed the presence of unmelted powder (Fig. 6.a). As already observed in LOM analyses, the Cu-4.3%Ag samples have higher bulk densities, however material discontinuities are still present and unmelted powder particles were found (Fig. 5.b and Fig. 6.b). The higher densities achieved with the coated powders are confirmed by SEM images in Fig. 5.c, Fig. 5.d, and Fig. 5.e. The microstructure of these materials is not homogeneous (Fig. 6.c) and is characterized by an Ag—Cu network among the partially melted Cu powder (Fig. 6.d) and a fully melted region exhibiting an eutectic structure (Fig. 6.g). EDX chemical analysis were performed to better identify the distribution of the elements, Cu is reported in orange, while Ag is depicted in light blue (Fig. 6.e and Fig. 6.f).

4. Discussion

4.1. Powder characterization

From the SEM images presented in Fig. 1, it is possible to observe that with by electrodeposition, a thin and uniform layer of Ag, with an approximate thickness of 300 nm, was homogeneously deposited on the surface of the pure Cu powder. To promote the diffusion of Cu in the

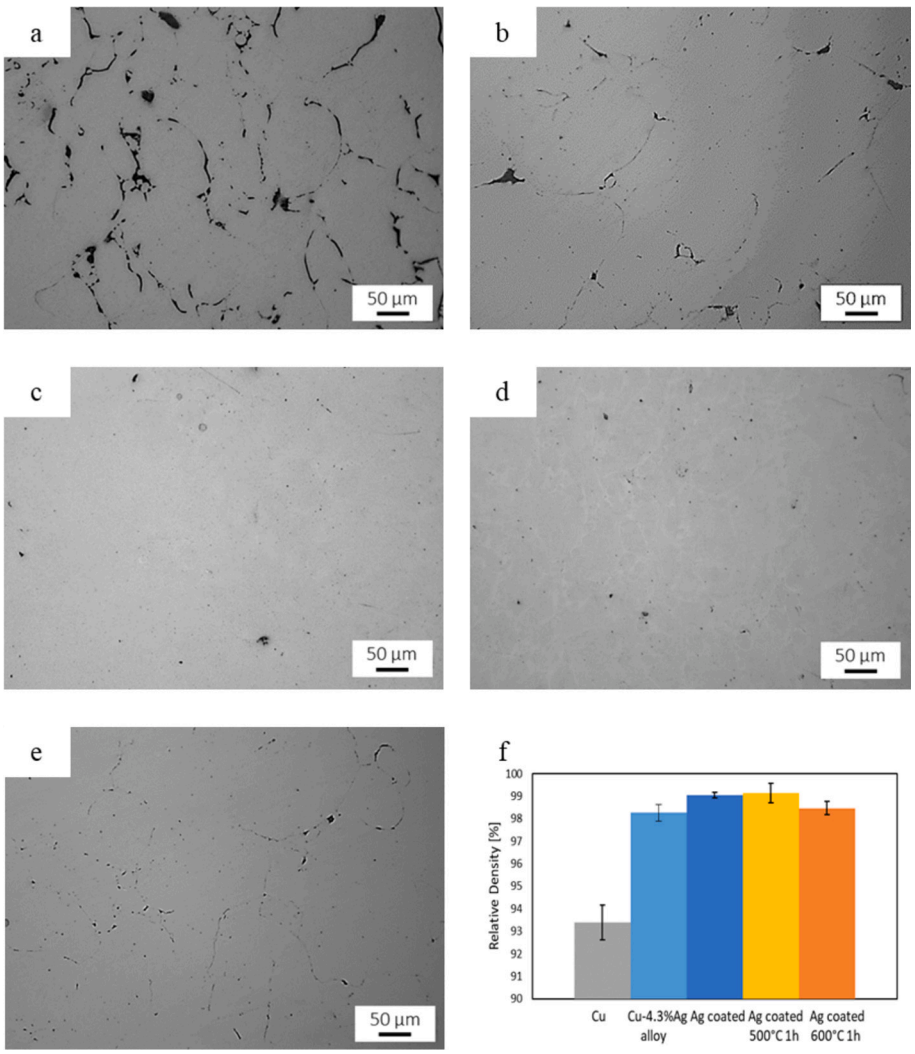

Fig. 4. Optical microscope images of samples produced with a) Cu powder, b) Cu-4.3%Ag alloy powder, c) Ag coated Cu powder, d) Ag coated Cu powder heat-treated at 500 °C for 1 h, e) Ag coated Cu powder heat-treated at 600 °C for 1 h, f) Relative density analysis performed with image analysis.

external Ag layer, the powder underwent heat treatment in a vacuum furnace following different schedules. This was aimed at evaluating the effect of different heat treatments and formation of different surface features on the absorptivity and processability of powder.

A first heat-treatment was performed at 500 °C for 1 h to promote the diffusion of Cu in the external layer. Indeed, sterling Ag, as recently proved, has excellent processability in the LPBF. Despite this alloy has similar properties compared to Cu, it has been demonstrated that high density final parts can be obtained by low power LPBF [31–33]. The heat treatment was performed to investigate the possible increase in processability given by the presence of a sterling Ag alloy only on the particles' surface. Given the mutual diffusion coefficients of the two elements Cu is expected to diffuse through Ag lattice more easily than Ag through Cu lattice [34,35]. After the heat treatment at 500 °C for 1 h, no discernible change in the morphology of the heat-treated powder compared to the initial state was observed (Fig. 1.i and Fig. 1.m). Due to the sub-micrometric size of the Ag layer, estimating the outward diffusion of Cu through SEM and EDS analysis proved challenging (Fig. 1.n and Fig. 1.o). However, a visual inspection of the powder color allowed for a qualitative evaluation of the heat-treatment effect. The Cu powder coated with Ag (Fig. 1.l) exhibited a grayish color typical of Ag. Following the heat treatment at 500 °C for 1 h, the powder displayed a pink color indicative of Cu outward diffusion (Fig. 1.p). For a more comprehensive assessment of Cu diffusion, XRD analyses were performed on the Ag-coated powder in the as-received and 500 °C heat-treated conditions. In Fig. 2, the Ag (111) peak of the heat-treated powder shifts toward higher angles, suggesting the migration of substitutional Cu atoms into the Ag layer. The diffusion of Cu atoms into the Ag lattice results in a contraction of the Ag lattice. This lattice contraction causes the Ag peaks to shift toward higher angles in the XRD pattern. This results in a contraction of the Ag lattice, causing a shift of the Ag peaks toward higher angles. Furthermore, the Ag peak of the heat-treated powder became asymmetrical, indicating the formation of a multi-layer compositional gradient which is likely richer in Cu nearby the interface.

The second heat-treatment was performed on the coated powders at 600 °C for 1 h to promote the formation of phase-segregated structure (heterostructures), in particular the effect of Ag dewetting from the surface of the powder was studied [36]. This segregation mechanism, driven by diffusion and lattice mismatch between Cu and Ag, has been reported in recent studies on electronic materials not related to AM, proposing it as a spontaneous dewetting process that leads to an interfacial energy reduction [37]. Regarding the SEM analysis performed on 600 °C heat-treated powder, it is possible to notice a change in the surface morphology of the powder (Fig. 1.q, Fig. 1.r, and Fig. 1.s). The Ag, originally uniformly distributed on the surface layer, merged into independent Ag groups over the Cu core. Visual inspection of the powder color revealed a darker pink color (Fig. 1.t), more similar to the color of

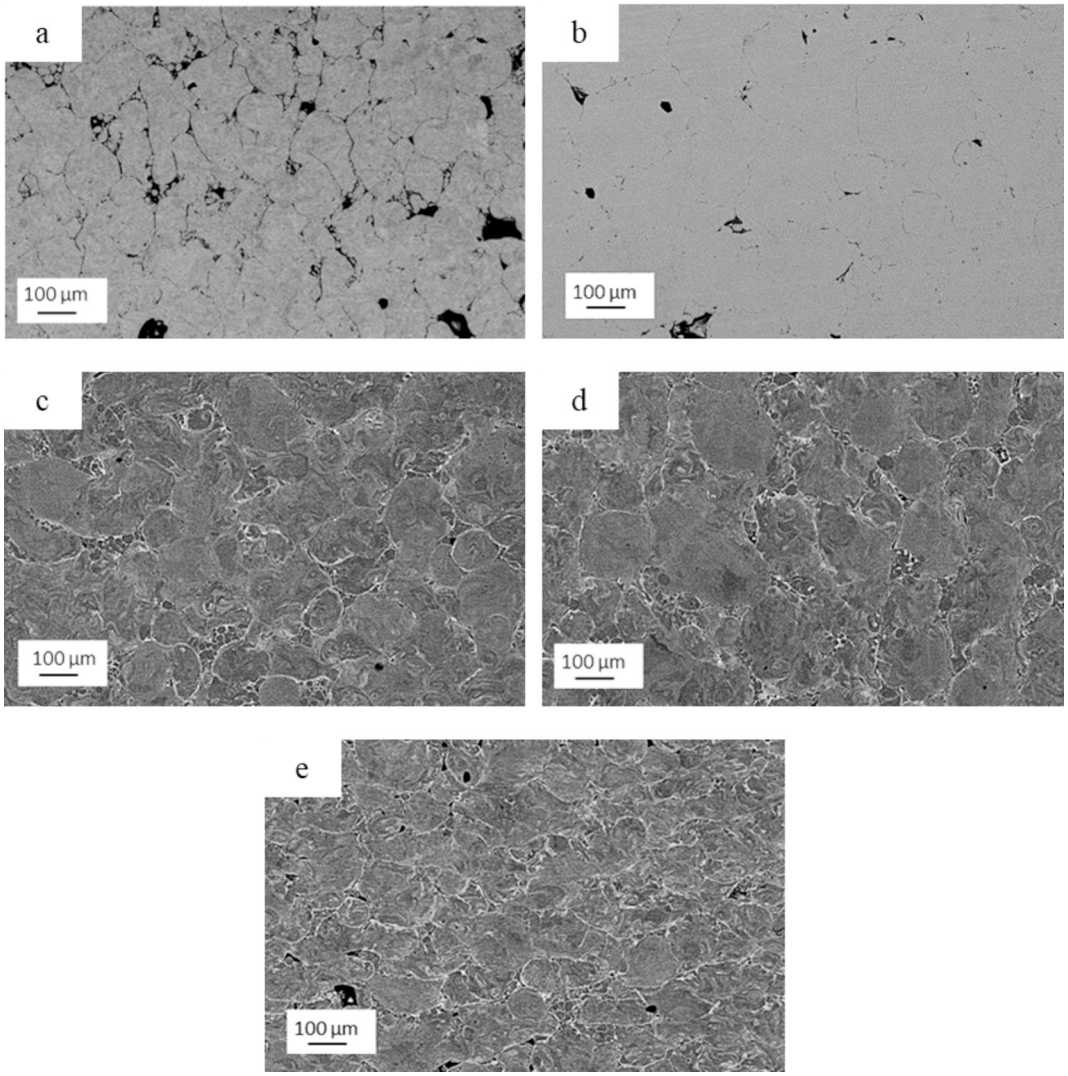

Fig. 5. SEM images of samples produced with a) Cu powder, b) Cu-4.3%Ag alloy powder, c) Ag coated Cu powder, d) Ag coated Cu powder heat-treated at 500 °C for 1 h, e) Ag coated Cu powder heat-treated at 600 °C for 1 h.

pure Cu powder (Fig. 1.d), due to the dewetting of the Ag layer and the formation of uncoated zones. A schematic of the effect of the heat treatment on the Ag-coated Cu particles found in this work has been proposed in Fig. 7.

The absorptivity of the different powder configurations was also investigated (Fig. 3). The analysis indicates that neither of the conducted heat-treatments effectively improved the laser absorption of the Cu powder. Indeed, no significant difference in absorbance at 1080 nm was observed for the Ag-coated Cu powder, the Cu-4.3%Ag, and the powder heat-treated at 600 °C compared to the pure Cu counterpart [7]. Minor variations in absorbance of the powder heat-treated at 500 °C was observed and could be attributed to slight differences in surface morphology and Cu concentration in Ag. The slight decrease in the absorbance of the laser could be explained by the changes in the surface morphology, as also reported in the work of Choi et al. for Ag-coated Cu nanoparticles for electronic applications [38]. They highlighted an intermediate step where the Ag layer becomes smoother before dewetting, a phenomenon widely reported in the literature to result in lower laser absorption due to a smoother powder surface [39].

4.2. Bulk characterization

The first sign of Ag effectiveness becomes apparent during the printing processes, where Cu samples exhibit a high delamination effect, while this phenomenon is notably absent in samples printed with Ag-containing powders, demonstrating superior processability. This enhanced processability is further confirmed by analyses performed on the cross-sections of bulk samples, revealing higher relative densities compared to those produced with pure Cu powder (Fig. 4).

For the pure Cu samples, LOM and SEM analyses showed partial melting with the presence of unmelted Cu particles (Fig. 5.a and Fig. 6.a). Additive-manufactured samples with Cu-4.3%Ag alloy powder exhibit a denser microstructure (Fig. 4.b and Fig. 5.b). However, the material displays non-uniform microstructure. Indeed, areas exhibiting complete fusion coexist with small voids within the fully melted zones, lack-of-fusion defects and partially melted powder particles (Fig. 6.b). Bulk materials produced with the coated powders in three different conditions show higher density than pure Cu and Cu-4.3%Ag alloy samples, emphasizing the effectiveness of functionalization (Fig. 4.f). The samples exhibited an uneven microstructure, with Ag distribution appearing non-uniform within specimens. The voids observed among fully melted areas in both Cu and Cu-4.3%Ag samples are now filled with Ag—Cu structures (Fig. 5). Original powder particles remain still distinguishable (Fig. 6.c and Fig. 6.d) but an Ag—Cu network formed between partially melted Cu particles. Such network consists of a Cu—Ag eutectic phase mixture that forms at the end of solidification and

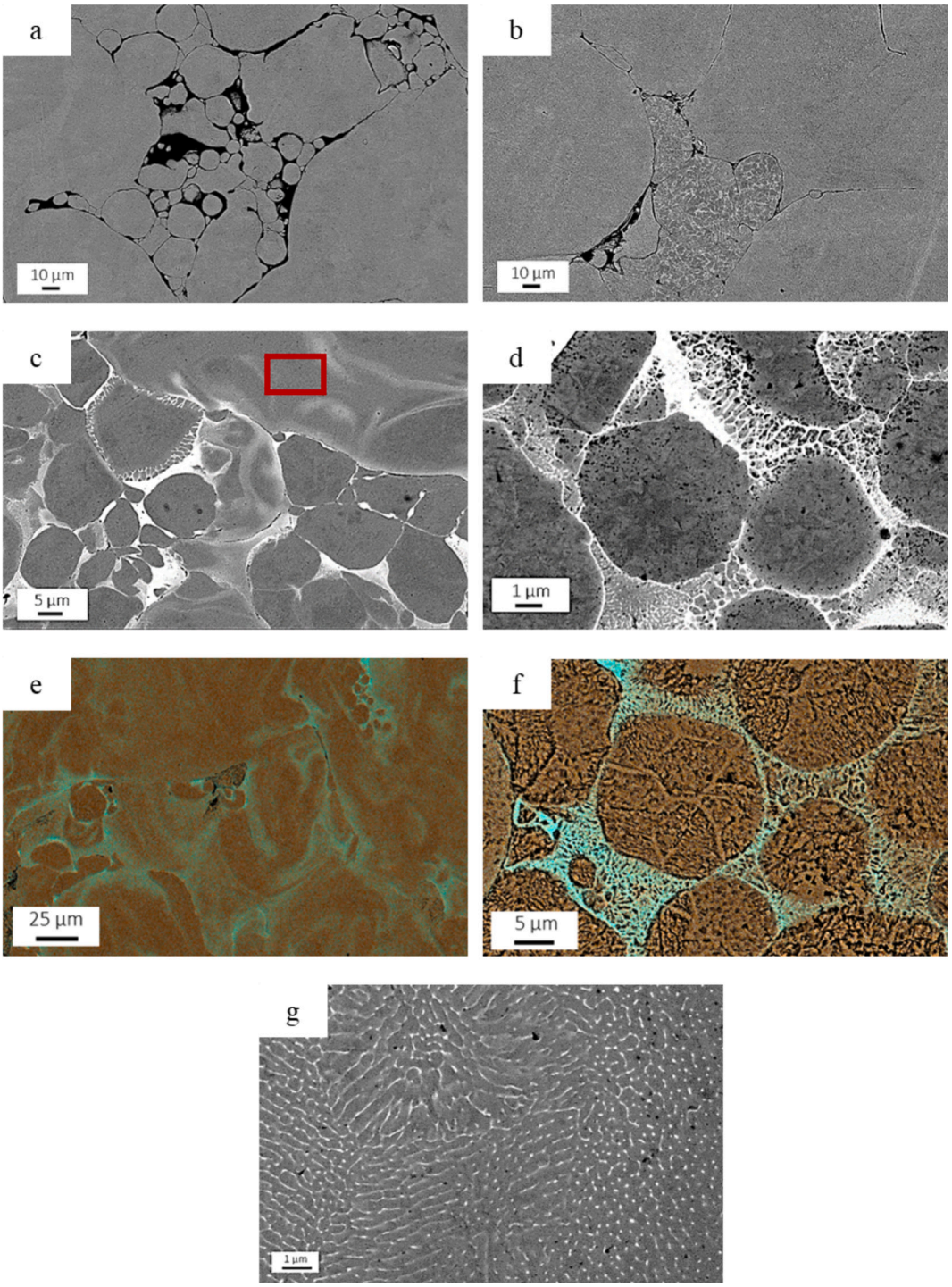

Fig. 6. SEM images of samples produced with a) pure Cu powder and b) Cu-4.3%Ag alloy powder, c), d), e) f), and g) Ag coated powder. e) and f) EDX chemical analysis (Cu and Ag are represented in orange and light blue, respectively.). f) SEM image at higher magnification of the region highlighted by the red square in c). (For interpretation of the references to color in this figure legend, the reader is referred to the web version of this article.)

possesses a healing ability as it fills the pores and defects within the partially melted Cu particles. SEM analysis at high magnification (Fig. 6. g) of the fully melted areas reveals the typical cellular-like solidification structure consisting of Cu cell decorated at boundaries by eutectic Ag particles. A schematic of the densification and healing mechanism proposed in this work is reported in Fig. 8.

Lastly, the relative densities of bulk materials obtained from the Ag-coated powder in as-received and heat-treated at 500 °C conditions are higher than in the case of samples produced from the functionalized powder heat-treated at 600 °C. This higher density can be attributed to the presence of a continuous Ag layer on the surface of the powder particles, facilitating the formation of an unbroken network between partially melted Cu particles. In the case of the powder heat-treated at 600 °C, the Ag layer is discrete due to the dewetting of Ag and the formation of heterostructures. A discontinuous layer resulted in a lower ability of Ag to heal pores and defects during solidification.

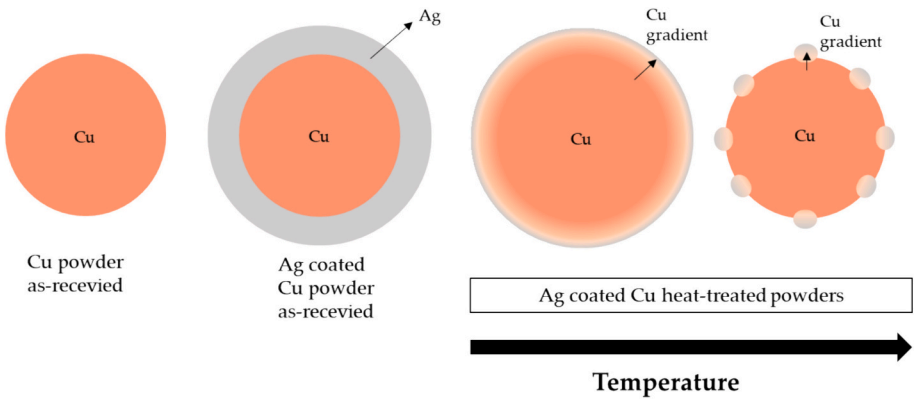

Fig. 7. Schematic behavior of heat-treated Ag coated Cu particles.

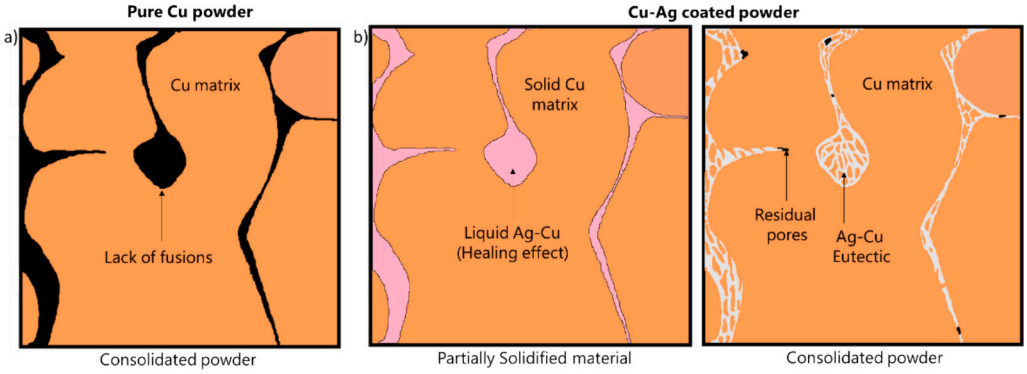

Fig. 8. Schematic representation of the proposed densification mechanism for the Ag coated powders.

5. Conclusions

In this study, an innovative approach to improve Cu processability by using a low-power (200 W) near-IR LPBF system was studied. This method is based on the Ag-coating of Cu particles that were heat-treated at 500 °C and 600 °C to promote diffusion at the coating interface and formation heterostructures. The functionalization of powders, with a thin and uniform layer of Ag, has resulted in remarkable improvements of the processability and densification of Cu powder. Microstructural analyses, including LOM and SEM examinations, highlighted different behaviors between pure Cu and Cu-4.3%Ag alloy samples. While the Cu-4.3%Ag alloy presented a denser microstructure, it also exhibited areas of incomplete fusion, small voids, and unmelted particles. However, when Ag coated powders were utilized, a notable improvement in material density was observed, and an Ag—Cu network formed between Cu particles, demonstrating the healing capability of the Ag during last stages of solidification. Heat treatment studies emphasized the importance of maintaining a continuous Ag layer for optimal density enhancement. The findings not only validate the efficacy of powder functionalization in improving material properties but also provide valuable insights into the mechanisms influencing the microstructural evolution during the additive manufacturing process.

CRediT authorship contribution statement

Giorgia Lupi: Writing – original draft, Investigation, Formal analysis, Data curation, Conceptualization. **Marcello Poulin:** Writing – review & editing, Investigation, Formal analysis. **Federico Gobber:** Writing – original draft, Methodology, Investigation, Formal analysis. **Marco Actis Grande:** Writing – review & editing, Supervision, Resources. **Riccardo Casati:** Writing – review & editing, Visualization, Validation, Supervision, Data curation, Conceptualization.

Declaration of competing interest

The authors declare that they have no known competing financial interests or personal relationships that could have appeared to influence the work reported in this paper.

Data availability

Data will be made available on request.

Acknowledgements

This study carried out within the MICS (Made in Italy – Circular and Sustainable) Extended Partnership and received funding from Next-GenerationEU (Italian PNRR – M4 C2, Invest 1.3 – D.D. 1551.11-10-2022, PE00000004).

Appendix A. Supplementary data

Supplementary data to this article can be found online at https://doi.org/10.1016/j.powtec.2024.120044.

References

[1] Q. Jiang, P. Zhang, Z. Yu, H. Shi, D. Wu, H. Yan, X. Ye, Q. Lu, Y. Tian, A review on additive manufacturing of pure copper, Coatings 11 (2021) 740, https://doi.org/10.3390/COATINGS11060740.
[2] S.D. Jadhav, L.R. Goossens, Y. Kinds, B. Van Hooreweder, K. Vanmeensel, Laser-based powder bed fusion additive manufacturing of pure copper, Addit. Manuf. 42 (2021) 101990, https://doi.org/10.1016/J.ADDMA.2021.101990.
[3] T. Mukherjee, J.S. Zuback, A. De, T. DebRoy, Printability of alloys for additive manufacturing, Sci. Rep. 6 (2016) 1–8, https://doi.org/10.1038/srep19717.

[4] J. Guan, X. Zhang, Y. Jiang, Y. Yan, Insights into fabrication mechanism of pure copper thin wall components by selective infrared laser melting, Rapid Prototyp. J. 25 (2019) 1388–1397, https://doi.org/10.1108/RPJ-06-2018-0143/FULL/PDF.
[5] X. Lingqin, C. Guang, Z. Luyu, L. Pan, Explore the feasibility of fabricating pure copper parts with low-laser energy by selective laser melting, Mater. Res. Express 7 (2020) 106509, https://doi.org/10.1088/2053-1591/ABBD08.
[6] C. Silbernagel, L. Gargalis, I. Ashcroft, R. Hague, M. Galea, P. Dickens, Electrical resistivity of pure copper processed by medium-powered laser powder bed fusion additive manufacturing for use in electromagnetic applications, Addit. Manuf. 29 (2019) 100831, https://doi.org/10.1016/J.ADDMA.2019.100831.
[7] H. Siva Prasad, F. Brueckner, J. Volpp, A.F.H. Kaplan, Laser metal deposition of copper on diverse metals using green laser sources, Int. J. Adv. Manuf. Technol. 107 (2020) 1559–1568, https://doi.org/10.1007/s00170-020-05117-z.
[8] E. Hori, Y. Sato, T. Shibata, K. Tojo, M. Tsukamoto, Development of SLM process using 200 W blue diode laser for pure copper additive manufacturing of high density structure, J. Laser Appl. 33 (2021) 12008, https://doi.org/10.2351/7.0000311/989464.
[9] M. Colopi, L. Caprio, A.G. Demir, B. Previtali, Selective laser melting of pure cu with a 1 kW single mode fiber laser, Proc. CIRP 74 (2018) 59–63, https://doi.org/10.1016/J.PROCIR.2018.08.030.
[10] F. Belelli, R. Casati, F. Larini, M. Riccio, M. Vedani, Investigation on two Ti–B-reinforced Al alloys for laser powder bed fusion, Mater. Sci. Eng. A 808 (2021) 140944, https://doi.org/10.1016/J.MSEA.2021.140944.
[11] F. Belelli, R. Casati, M. Vedani, J. Volpp, Design and characterization of Al–Mg–Si–Zr alloys with improved laser powder bed fusion processability, Metall. Mater. Trans. A 53 (2021) 331–343, https://doi.org/10.1007/S11661-021-06531-Y.
[12] P. Lassègue, C. Salvan, E. De Vito, R. Soulas, M. Herbin, A. Hemberg, T. Godfroid, T. Baffie, G. Roux, Laser powder bed fusion (L-PBF) of Cu and CuCrZr parts: influence of an absorptive physical vapor deposition (PVD) coating on the printing process, Addit. Manuf. 39 (2021), https://doi.org/10.1016/J.ADDMA.2021.101888.
[13] Z. Ma, K. Zhang, Z. Ren, D.Z. Zhang, G. Tao, H. Xu, Selective laser melting of Cu–Cr–Zr copper alloy: parameter optimization, microstructure and mechanical properties, J. Alloys Compd. 828 (2020) 154350, https://doi.org/10.1016/J.JALLCOM.2020.154350.
[14] K. Jahns, R. Bappert, P. Böhlke, U. Krupp, Additive manufacturing of CuCr1Zr by development of a gas atomization and laser powder bed fusion routine, Int. J. Adv. Manuf. Technol. 107 (2020) 2151–2161, https://doi.org/10.1007/S00170-020-04941-7/FIGURES/12.
[15] X. Yang, Y. Qi, W. Zhang, Y. Wang, H. Zhu, Laser powder bed fusion of C18150 copper alloy with excellent comprehensive properties, Mater. Sci. Eng. A 862 (2023) 144512, https://doi.org/10.1016/J.MSEA.2022.144512.
[16] A.P. Ventura, C.A. Wade, G. Pawlikowski, M. Bayes, M. Watanabe, W.Z. Misiolek, Mechanical properties and microstructural characterization of Cu-4.3 Pct Sn fabricated by selective laser melting, Metall. Mater. Trans. A 48 (2017) 178–187, https://doi.org/10.1007/s11661-016-3779-x.
[17] J. Yin, W. Zhang, L. Ke, H. Wei, D. Wang, L. Yang, H. Zhu, P. Dong, G. Wang, X. Zeng, Vaporization of alloying elements and explosion behavior during laser powder bed fusion of Cu–10Zn alloy, Int. J. Mach. Tools Manuf. 161 (2021) 103686, https://doi.org/10.1016/j.ijmachtools.2020.103686.
[18] S. Uchida, T. Kimura, T. Nakamoto, T. Ozaki, T. Miki, M. Takemura, Y. Oka, R. Tsubota, Microstructures and electrical and mechanical properties of Cu-Cr alloys fabricated by selective laser melting, Mater. Des. 175 (2019) 107815, https://doi.org/10.1016/J.MATDES.2019.107815.
[19] Y. Chen, S. Ren, Y. Zhao, X. Qu, Microstructure and properties of CuCr alloy manufactured by selective laser melting, J. Alloys Compd. 786 (2019) 189–197, https://doi.org/10.1016/J.JALLCOM.2019.01.179.
[20] S. Zhang, H. Zhu, L. Zhang, W. Zhang, H. Yang, X. Zeng, Microstructure and properties of high strength and high conductivity Cu-Cr alloy components fabricated by high power selective laser melting, Mater. Lett. 237 (2019) 306–309, https://doi.org/10.1016/J.MATLET.2018.11.118.
[21] G. Zhang, C. Chen, X. Wang, P. Wang, X. Zhang, X. Gan, K. Zhou, Additive manufacturing of fine-structured copper alloy by selective laser melting of pre-alloyed Cu-15Ni-8Sn powder, Int. J. Adv. Manuf. Technol. 96 (2018) 4223–4230, https://doi.org/10.1007/s00170-018-1891-3.
[22] V. Lindström, O. Liashenko, K. Zweiacker, S. Derevianko, V. Morozovych, Y. Lyashenko, C. Leinenbach, Laser powder bed fusion of metal coated copper powders, Materials 13 (2020) 3493, https://doi.org/10.3390/MA13163493.
[23] Z. Hu, B. Gan, J. Tan, J. Wu, S. Chen, J. Dong, Z. Ma, The enhancement of laser absorptivity and properties in laser powder bed fusion manufactured Cu-Cr-Zr alloy by employing Y2O3 coated powder as precursor, J. Alloys Compd. 927 (2022) 167111, https://doi.org/10.1016/J.JALLCOM.2022.167111.
[24] S.D. Jadhav, D. Fu, M. Deprez, K. Ramharter, D. Willems, B. Van Hooreweder, K. Vanmeensel, Highly conductive and strong CuSn0.3 alloy processed via laser powder bed fusion starting from a tin-coated copper powder, Addit. Manuf. 36 (2020) 101607, https://doi.org/10.1016/J.ADDMA.2020.101607.
[25] R. Zheng, J. Cui, Y. Yang, S. Li, R.D.K. Misra, K. Kondoh, Q. Zhu, Y. Lu, X. Li, Enhanced densification of copper during laser powder bed fusion through powder surface alloying, J. Mater. Process. Technol. 305 (2022) 117575, https://doi.org/10.1016/J.JMATPROTEC.2022.117575.
[26] Y. Sakai, K. Inoue, T. Asano, H. Wada, H. Maeda, Development of high-strength, high-conductivity Cu–Ag alloys for high-field pulsed magnet use, Appl. Phys. Lett. 59 (1991) 2965–2967, https://doi.org/10.1063/1.105813.
[27] H.Y. Yang, Z.C. Ma, C.H. Lei, L. Meng, Y.T. Fang, J. Bin Liu, H.T. Wang, High strength and high conductivity Cu alloys: a review, Sci. China Technol. Sci. 63 (2020) 2505–2517, https://doi.org/10.1007/S11431-020-1633-8/METRICS.
[28] X. Zhu, Z. Xiao, J. An, H. Jiang, Y. Jiang, Z. Li, Microstructure and properties of Cu-Ag alloy prepared by continuously directional solidification, J. Alloys Compd. 883 (2021) 160769, https://doi.org/10.1016/J.JALLCOM.2021.160769.
[29] Kymera International - Pioneers in Material Science, (n.d.). https://www.kymerainternational.com/ (accessed January 15, 2024).
[30] X. Xu, X. Luo, H. Zhuang, W. Li, B. Zhang, Electroless silver coating on fine copper powder and its effects on oxidation resistance, Mater. Lett. 57 (2003) 3987–3991, https://doi.org/10.1016/S0167-577X(03)00252-0.
[31] W. Xiong, L. Hao, Y. Li, D. Tang, Q. Cui, Z. Feng, C. Yan, Effect of selective laser melting parameters on morphology, microstructure, densification and mechanical properties of supersaturated silver alloy, Mater. Des. 170 (2019) 107697, https://doi.org/10.1016/J.MATDES.2019.107697.
[32] W. Xiong, L. Hao, T. Peijs, C. Yan, K. Cheng, P. Gong, Q. Cui, D. Tang, S. Al Islam, Y. Li, Simultaneous strength and ductility enhancements of high thermal conductive Ag7.5Cu alloy by selective laser melting, Sci. Rep. 12 (2022) 1–15, https://doi.org/10.1038/s41598-022-08182-4.
[33] R.J. Vikram, L. Kollo, K.G. Prashanth, S. Suwas, Investigating the structure, microstructure, and texture in selective laser-melted Sterling silver 925, Metall. Mater. Trans. A 52 (2021) 5329–5341, https://doi.org/10.1007/s11661-021-06471-7.
[34] A. Ceylan, K. Jastrzembski, S.I. Shah, Enhanced solubility ag-cu nanoparticles and their thermal transport properties, Metall. Mater. Trans. A Phys. Metall. Mater. Sci. 37 (2006) 2033–2038, https://doi.org/10.1007/BF02586123/METRICS.
[35] D.B. Butrymowicz, J.R. Manning, M.E. Read, Diffusion in copper and copper alloys, part II. Copper-silver and copper-gold systems, J. Phys. Chem. Ref. Data 3 (1974) 527–602, https://doi.org/10.1063/1.3253145.
[36] S.J. Kim, E.A. Stach, C.A. Handwerker, Fabrication of conductive interconnects by Ag migration in Cu-Ag core-shell nanoparticles, Appl. Phys. Lett. 96 (2010) 144101, https://doi.org/10.1063/1.3364132/986639.
[37] Z.Z. Fang, H. Wang, Densification and grain growth during sintering of nanosized particles, Int. Mater. Rev. 53 (2008) 326–352, https://doi.org/10.1179/174328008X353538.
[38] E.B. Choi, J.H. Lee, Dewetting behavior of Ag in Ag-coated Cu particle with thick Ag shell, Appl. Surf. Sci. 480 (2019) 839–845, https://doi.org/10.1016/J.APSUSC.2019.02.221.
[39] B. Brandau, A. Da Silva, C. Wilsnack, F. Brueckner, A.F.H. Kaplan, Absorbance study of powder conditions for laser additive manufacturing, Mater. Des. 216 (2022) 110591, https://doi.org/10.1016/J.MATDES.2022.110591.